Intervening Nidal Brain Parenchyma and Risk of Radiation-Induced Changes After Radiosurgery for Brain Arteriovenous Malformation: A Study Using an Unsupervised Machine Learning Algorithm

Cheng-Chia Lee[1,4,5], Huai-Che Yang[1,4], Chung-Jung Lin[2,4], Ching-Jen Chen[6], Hsiu-Mei Wu[2,4], Cheng-Ying Shiau[2,3], Wan-Yuo Guo[2,4], David Hung-Chi Pan[1,4,9], Kang-Du Liu[1,4], Wen-Yuh Chung[1,4], Syu-Jyun Peng[7,8]

OBJECTIVE: **To assess the sensitivity and specificity of arteriovenous malformation (AVM) nidal component identification and quantification using an unsupervised machine learning algorithm and to evaluate the association between intervening nidal brain parenchyma and radiation-induced changes (RICs) after stereotactic radiosurgery.**

METHODS: **Fully automated segmentation via unsupervised classification with fuzzy c-means clustering was used to analyze the AVM nidus on T2-weighted magnetic resonance imaging studies. The proportions of vasculature, brain parenchyma, and cerebrospinal fluid were quantified. These were compared with the results from manual segmentation. The association between the brain parenchyma component and RIC development was assessed.**

RESULTS: **The proposed algorithm was applied to 39 unruptured AVMs in 39 patients (17 female and 22 male patients), with a median age of 27 years. The median proportion of the constituents was as follows: vasculature, 31.3%; brain parenchyma, 48.4%; and cerebrospinal fluid, 16.8%. RICs were identified in 17 of the 39 patients (43.6%). Compared with manual segmentation, the automated algorithm was able to achieve a Dice similarity index of 79.5% (sensitivity, 73.5%; specificity, 85.5%). RICs were associated with a greater proportion of intervening nidal brain parenchyma (52.0% vs. 45.3%; $P = 0.015$). Obliteration was not associated with greater proportions of nidal vasculature (36.0% vs. 31.2%; $P = 0.152$).**

CONCLUSIONS: **The automated segmentation algorithm was able to achieve classification of the AVM nidus components with relative accuracy. Greater proportions of intervening nidal brain parenchyma were associated with RICs.**

INTRODUCTION

Stereotactic radiosurgery (SRS) is an effective treatment option for select cases of brain arteriovenous malformations (AVMs).[1] With the increasing popularity of SRS for AVMs with small- to medium-size nidi located in deep or eloquent regions of the brain, efforts to characterize and prevent treatment-specific complications have become crucial.[1-5] Adverse radiation effects (AREs) after SRS for AVMs have included cyst formation and radiation-induced changes (RICs).[6,7] Delayed cyst formation will occur in ~3% of patients with AVM who have undergone SRS after a mean latency period of 6.5 years, and approximately one third of these patients will require surgical

Key words
- Adverse radiation effects
- Arteriovenous malformation
- Fuzzy c-means
- Gamma knife radiosurgery
- Image analysis
- Radiation-induced changes
- Stereotactic radiosurgery

Abbreviations and Acronyms
ARE: Adverse radiation effect
AVM: Arteriovenous malformation
CI: Confidence interval
CSF: Cerebrospinal fluid
FCM: Fuzzy c-means
FSE: Fast spin echo
MRA: Magnetic resonance angiography
MRI: Magnetic resonance imaging
OR: Odds ratio
RIC: Radiation-induced change
ROI: Region of interest
SRS: Stereotactic radiosurgery

From the [1]Department of Neurosurgery, Neurological Institute, [2]Department of Radiology, and [3]Cancer Center, Taipei Veterans General Hospital, Taipei, Taiwan; [4]School of Medicine, and [5]Brain Research Center, National Yang-Ming University, Taipei, Taiwan; [6]Department of Neurological Surgery, University of Virginia Health System, Charlottesville, Virginia, USA; and [7]Biomedical Electronics Translational Research Center and [8]Institute of Electronics, National Chiao Tung University, Hsin-Chu, Taiwan; and [9]Department of Neurosurgery, Shuang Ho Hospital, Taipei Medical University, Taipei, Taiwan

To whom correspondence should be addressed: Syu-Jyun Peng, Ph.D. [E-mail: blue.year@msa.hinet.net]

Citation: World Neurosurg. (2019) 125:e132-e138. https://doi.org/10.1016/j.wneu.2018.12.220

Journal homepage: www.journals.elsevier.com/world-neurosurgery

Available online: www.sciencedirect.com

intervention.[7] RICs have been the most frequently observed complications, with latency periods ranging from 6 to 18 months after SRS for AVMs.[8-15] Although most RICs will be asymptomatic, a subset of patients will develop neurological symptoms.[1,6,9,12-15] Although most symptomatic RICs will be transient and can be managed medically, a few patients will experience a permanent neurological deficit after AVM treatment.[6]

The risk factors for RICs after SRS for AVMs include a deep AVM location, large radiation treatment volume, history of AVM rupture, and high margin or maximum radiation dose.[1,10,11,14,16-24] Although volume- or dose-staged SRS has been used for AVMs with large volumes, compared with AVMs with a diffuse or large-volume nidus, those with a small, compact nidus have been considered to be more amenable to SRS.[25,26] The correlation between AVM treatment volume and RICs might be associated with the intervening nidal brain parenchyma.[1,13,19,27] Hence, the goals of the present study were 1) to assess the sensitivity and specificity of AVM nidal component identification and quantification using an unsupervised machine learning algorithm; and 2) to evaluate the association between the intervening nidal brain parenchyma and RICs after SRS.

METHODS

Patient Selection

From January 2000 to December 2013, 584 patients underwent SRS for AVMs at our institution. The patient demographic, clinical, neuroimaging, and SRS data from a prospectively maintained, institutional review board–approved database were retrospectively reviewed. For inclusion in the present study, the following criteria were used: 1) unruptured AVMs treated with SRS; 2) AVMs with a medium volume of 3–5 cm^3; and 3) clinical and neuroimaging follow-up data available for ≥3 years. Patients who had undergone previous AVM treatment, including external beam radiotherapy, SRS, microsurgical resection, and endovascular embolization, were excluded from the present study.

Radiosurgical Technique

The SRS technique used in the present study has been previously described.[28-31] In brief, the Leksell model G frame (Elekta AB, Stockholm, Sweden) was affixed to the patient's head with the patient under local or monitored anesthesia. Digital subtraction angiography and thin-slice, volumetric magnetic resonance imaging (MRI) with contrast enhancement were performed to delineate the angioarchitecture and spatial anatomy of the AVM nidus. SRS was performed using the Leksell Gamma Unit model 3C from 2000 to 2014, Leksell Gamma Unit model 4C from 2007 to 2014, and the Perfexion model (Elekta, AB, Stockholm, Sweden) thereafter. Radiosurgical parameters and dose plans were formulated by the treating neurosurgeon in consultation with a medical physicist and radiation oncologist.

Follow-Up Protocol

Neuroimaging, consisting of MRI and magnetic resonance angiography (MRA), was performed routinely at ~6-month intervals after SRS. All MRI and MRA studies were performed using the Signa HDxt 1.5T magnetic resonance scanner (GE Healthcare, Milwaukee, Wisconsin, USA) equipped with an 8-channel phased-array neurovascular coil. The sequences acquired included T1-weighted gradient echo with and without contrast enhancement, T2-weighted fast spin echo (FSE; repetition time, 4000–5500 ms; echo time, 80–100 ms; field of view, 260 mm; number of excitations, 2; slice thickness, 3 mm; slice gap, 3 mm) and 3-dimensional time of flight (repetition time, 6.9 ms; echo time, 45 ms; field of view, 260 mm; number of excitations, 2; slice thickness, 1.5–2 mm; slice gap, 1.5–2 mm). The MRI and MRA protocols at our institution remained relatively constant throughout the study period, with only slight changes resulting from improvements in MRI technology.

AVM obliteration was defined by the lack of flow voids on the T2-weighted FSE sequence or the disappearance of abnormal arteriovenous shunting on digital subtraction angiography. RICs were defined as perinidal hyperintensities on T2-weighted FSE sequences and were categorized according to the grading system developed by Yen et al.[32] Grade I RICs were defined as mild imaging changes with <10 mm of increased T2 signal surrounding the treated AVM nidus and no mass effect. Grade II RICs were defined as moderate imaging changes with ≥10 mm of increased T2 signal and a mild to moderate mass effect resulting in sulcal effacement or ventricular compression. Grade III RICs were defined as severe imaging changes with a midline shift of the brain.

Automated Segmentation Procedure

An automated segmentation algorithm for AVM nidal component identification and quantification was developed using unsupervised machine learning with fuzzy c-means (FCM) clustering.[33,34] The analysis was performed on the AVM nidus as delineated on T2-weight FSE images in the SRS dose plan. The algorithm was implemented using MATLAB (MathWorks, Inc., Natick, Massachusetts, USA) on a moderate-performance computer. The image analysis and automated segmentation procedures included the 4 steps outlined below:

Step 1: Region of interest (ROI) definition

Linear interpolation was used to convert the dose intensity distribution in the dose plan map into the corresponding spatial positions on T2-weighted images. After radiation dose intensity selection (i.e., 100% isodose; unit, centiGray), the radiation exposure regions on the T2-weighted images were defined as a dose intensity equal to or greater than the previously selected radiation dose intensity. The ROI was defined as the radiation exposure region.

Step 2: FCM classification

Voxels within the ROI of the T2-weighted images were classified into different tissue types using FCM clustering. The voxels were classified into 3 clusters (nidus, brain, and cerebrospinal fluid [CSF]) according to the distribution characteristics of the voxel intensity (**Figure 1**).

Step 3: Calculations of volumes or proportions

The volumes and proportions of each tissue type (i.e., nidus, brain, and CSF) within the ROI were automatically calculated.

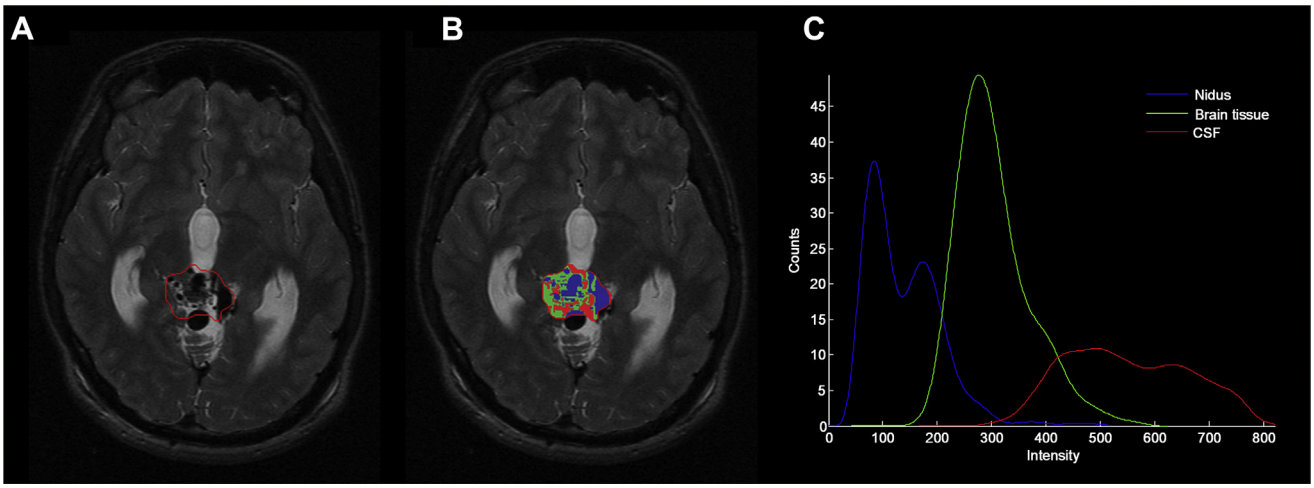

Figure 1. Histographic characterization of a brain arteriovenous malformation. Intensity histograms of T2-weighted image within region exposed to radiation of 1 patient in the present study. Manually demarcated regions include nidus (*dark blue*), brain tissue (*green*), and cerebrospinal fluid (CSF) (*red*). (**A**) *Red curve* indicates region exposed to radiation. (**B**) *Blue, green,* and *red* denote nidus, brain tissue, and CSF of manual segmentation, respectively. (**C**) Intensity histogram of nidus, brain tissue, and CSF from manual segmentation within region exposed to radiation.

Step 4: Validation

The results of automatic segmentation using FCM clustering results were compared with those obtained using manual segmentation by 2 of us (H.C.Y. and C.C.L.).

Statistical Analysis

All statistical analyses were performed using SPSS, version 20.0 (IBM Corp., Armonk, New York, USA). Descriptive statistics are presented as the median and range for all continuous variables, and as frequencies and percentages for categorical variables. Univariate comparisons of continuous variables were performed using the independent Student t test. Statistical significance was defined as a P value of < 0.05, and all tests of significance were 2-tailed.

RESULTS

Patient Cohort

The study cohort comprised 39 patients who had satisfied the inclusion criteria. The demographic, clinical, neuroimaging, and SRS data for the study cohort are listed in **Table 1**. Of the 39 patients, 22 were male and 17 were female, with a median age of 27 years (range, 8–77). All AVMs were unruptured and had a medium volume of 3–5 cm^3. All AVMs had a Spetzler-Martin grade of I–III and were in various locations. The median neuroimaging and clinical follow-up examinations were performed at 45 months (range, 36–144) and 53 months (range, 36–171), respectively. The median margin dose was 19 Gy (range, 15–22), and the median maximal dose was 32 Gy (range, 25–35).

The characteristics of RICs observed in the study cohort are listed in **Table 2**. No RICs were observed in 22 patients. Grades I and II RICs were found in 14 and 3 patients, respectively. No grade III RICs were observed, and no patient died in the present study.

Validation of Automatic Segmentation Results

The results of automatic segmentation using FCM clustering were compared with those obtained using manual segmentation. A case example of segmentation results obtained using FCM and manual clustering is shown in **Figure 2**. Automatic segmentation using an unsupervised FCM machine learning algorithm was able to achieve a segmentation Dice similarity index of 79.5%, with a sensitivity and specificity of 73.5% and 85.5%, respectively, compared with manual clustering.

RICs and Intervening Nidal Brain Parenchyma Component

The proportions of nidus, brain, and CSF were 31.3%, 48.4%, and 16.8% among the 39 AVMs in the study cohort, respectively, using automatic segmentation and FCM clustering. The association between the RICs and intervening nidal brain parenchyma component is shown in **Figure 3A**. Patients with RICs after SRS for AVMs had significantly greater proportions of intervening nidal brain parenchyma compared with those without RICs (52.0% $\pm$ 7.6% vs. 45.3% $\pm$ 8.6%; $P = 0.015$).

Regarding the severity and period of RICs, 14 patients had grade I RIC and 3 had grade II RIC. The median interval between gamma knife radiosurgery and the first RIC was 6 months (range, 3–27) in these 17 patients. The median period of RIC was 12 months (range, 8–39) in these 17 patients. No relationship was found between the degree of the brain tissue component and the onset and duration of RICs.

AVM Obliteration and Vascular Nidal Component

The association between AVM obliteration and the proportion of vascular tissue within the nidus is shown in **Figure 3B**. Complete obliteration was achieved in 29 of the 39 AVMs (74.3%) treated with SRS. The proportions of nidal vascular tissue were

Table 1. Demographic, Clinical, Neuroimaging, and Stereotactic Radiosurgery Data

Characteristic	*n* (%)
Sex	
Male	22
Female	17
Age (years)	
Median	27
Range	8–77
AVM diameter (cm)	
Median ± standard deviation	2.1 ± 2.0
Range	1–3
Deep vein drainage	
Yes	22
No	17
Eloquent area	
Yes	20
No	19
Spetzler-Martin grade	
I	15
II	15
III	9
Neuroimaging follow-up (months)	
Median ± standard deviation	45 ± 51
Range	36–114
Clinical follow-up (months)	
Median ± standard deviation	53 ± 58
Range	36–171
AVM volume (cm^3)	
Median ± standard deviation	4.2 ± 4.2
Range	3.0–5.0
Margin dose (Gy)	
Median ± standard deviation	19 ± 19
Range	15–22
Maximal dose (Gy)	
Median ± standard deviation	32 ± 31
Range	26–35
Isodose line (%)	
Mean ± standard deviation	60 ± 60
Range	55–65

AVM, arteriovenous malformation.

Table 2. Radiation-Induced Changes Compared with Brain Tissue Component

RICs Found on Imaging Study	Patients (*n*, %)
None	22 (56)
Yes	
Grade I	14 (36)
Grade II	3 (8)
Grade III	0 (0)
Mortality	0 (0)

RICs, radiation-induced changes.

comparable between AVMs with obliteration and those without obliteration after SRS (32.8% ± 10.8% vs. 37.2% ± 8.5%; P = 0.242).

DISCUSSION

Mechanisms of RICs

AREs after SRS for AVMs have included RICs, cyst formation, radiation necrosis, and encapsulated hematoma formation.[9,29,35] RICs have been the most frequently observed complications and can be associated with transient or permanent neurological symptoms.[8-15] These complications are readily recognized as perinidal T2 hyperintensities or contrast enhancement on MRI, resulting from blood–brain barrier breakdown.[1,9] To achieve AVM obliteration, SRS induces endothelial damage, which leads to the proliferation of smooth muscle cells and the formation of extracellular collagen, and subsequent progressive vascular stenosis.[29,36,37] The extent of these vascular changes can vary among individual AVMs. Irradiation of susceptible AVMs with fragile telangiectatic perinidal vasculature can result in serum and protein exudation, leading to formation of RICs, cysts, or encapsulated hematomas.[29,35,36] Radiation necrosis can develop in severe cases and has been associated with a variety of factors, including secondary injury via inflammatory mediators, direct glial injury, and perivascular lymphocyte infiltration.[14,38] Despite the lack of essential neurological function, the intervening nidal brain parenchyma often included within the radiation treatment volume might play an important role in ARE development. This nonfunctional intervening brain parenchyma can cause delayed complications, resulting in vasogenic edema and immune reactions.

A number of demographic, AVM, and treatment characteristics have been suggested as risk factors for ARE development after SRS for AVMs.[1,10,11,14,16-24] In a recent meta-analysis of pooled data from 51 studies, Ilyas et al.[6] found unruptured AVMs (odds ratio [OR], 0.57; 95% confidence interval [CI], 0.47–0.69; P < 0.0001) and repeat SRS (OR, 6.19; 95% CI, 2.42–2.64; P = 0.0001) were significant risk factors for the development of RICs. In the same study, they found a deep AVM location (OR, 0.38; 95% CI, 0.21–0.67; P = 0.0009) to be a significant risk factor for symptomatic RICs after SRS. Several retrospective studies have also shown that the development of RICs is related to the radiation dose and volume, especially the

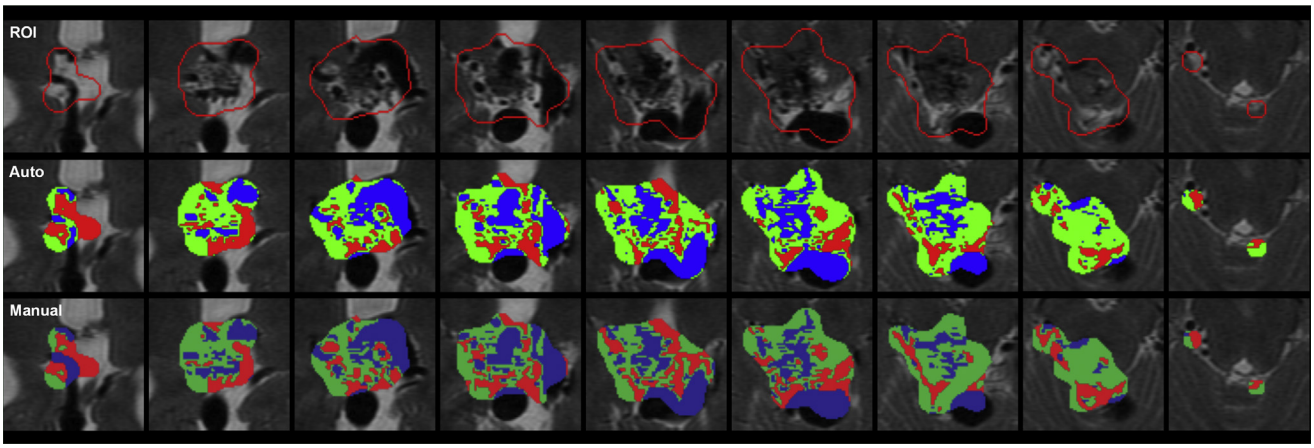

Figure 2. Region of interest (ROI) exposed to radiation, manual segmentation, and automated segmentation in T2-weighted images from an illustrative case. *Red curve* indicates boundary of 100% isodose region. *Blue, green,* and *red* denote nidus, brain tissue, and cerebrospinal fluid, respectively.

nidus volume. To prevent the bias, we enrolled the patients who had had an AVM of 3–5 cm^3 and a margin dose of 15–22 Gy. We excluded large AVMs >5 cm^3 and those receiving a large dose >25 Gy to minimize the effects of prescription dose and target volume on the outcomes. Therefore, no correlation was present between the RIC and the radiation dose and AVM volume. Despite radiation dose optimization, precise nidus delineation, and a conforming radiosurgical dose plan, RICs could not be completely prevented owing to the intervening nidal brain parenchyma.

However, the obliteration of the AVM was not associated with a greater proportion of the vascular component (36.0% vs. 31.2%; P = 0.152) included in the target. The reason for the poor correlation is unknown. However, the successful obliteration of an AVM after gamma knife SRS has generally been thought to result from the proliferation of smooth muscle cells and elaboration of extracellular collagen by these cells,[36] not simply to the nidal vessels within the target. Therefore, a greater incidence of shunting vessels and longer nidal vessels were not related to a greater rate of obliteration. However, a larger patient population would be necessary for more solid evidence.

Importance of AVM Nidal Component Quantification

A general expectation exists that compact AVMs will have better response to SRS than will diffuse AVMs owing to the assumption that the high density of the nidal vasculature will allow for radiation concentration within the small treatment volume. However, the definitions of "compactness" or "diffuseness" have remained subjective, because manual voxel-by-voxel quantification of the

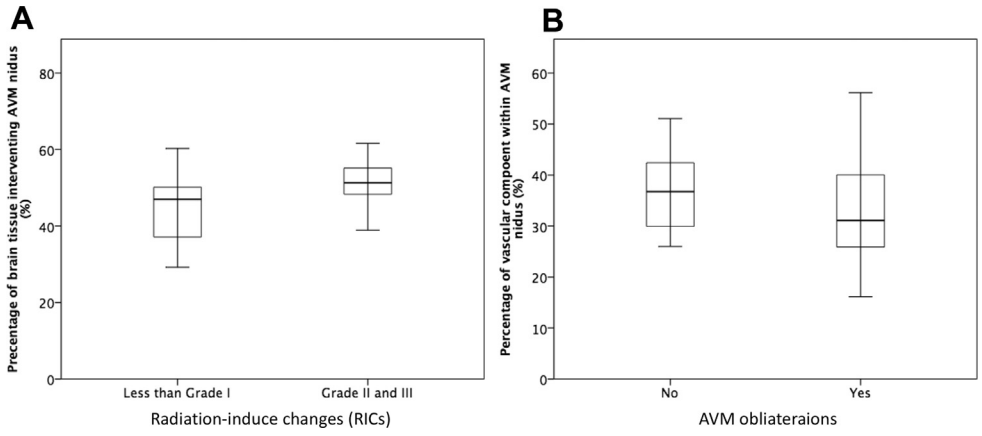

Figure 3. (**A**) Box plot demonstrating significant association between radiation-induced changes (RICs) and brain tissue component of arteriovenous malformation (AVM) nidus. Patients with more brain tissue components were prone to RICs after radiosurgery ($P = 0.015$). (**B**) Box plot demonstrating association between complete obliteration and percentage of vascular components within brain AVM nidus ($P = 0.242$).

AVM nidus can be painstakingly time-consuming and impractical. Hence, the development of an automated process could help to facilitate the quantification and provide an objective definition of "compactness." In the present preliminary study, we used unsupervised machine learning to differentiate and quantify the AVM nidal composition. The automated segmentation algorithm uses FCM clustering to group data with similar characteristics into clusters according to the distribution of data and then analyzing the data clusters separately. This is in contrast to supervised machine learning, which provides a priori definitions that indicate the meaning of the clusters. Unsupervised machine learning groups data with similar characteristics using clustering techniques. Next, the meaning of each cluster is analyzed and defined. Using this technique to analyze the AVM nidal composition makes it possible to eliminate the bias that can result from using absolute values to define grayscale images, such as blood vessels, brain tissue, and CSF on MRI scans. It also eliminates the need for control group comparisons on MRI scans.

Machine learning depends largely on classification algorithms, including support vector machines, boosted and bagged decision trees, K-nearest neighbor, naive Bayes classifiers, discriminant analysis, logistic regression, and neural networks. Clustering algorithms include k-means, k-medoids, hierarchical clustering, Gaussian mixture models, hidden Markov models, self-organizing maps, FCM, and subtractive clustering. In the present study, we selected an unsupervised clustering method, fuzzy c-means, because AVMs contain 3 major structures, which are best managed using clustering rather than classification. Moreover, AVM image segmentation performed by different radiologists is unlikely to produce identical results; thus, it has been difficult to formulate a reference standard. Therefore, we selected FCM, which does not require marking beforehand. Future research is required to determine whether hierarchical clustering or a mixture of Gaussian models could also be used for AVM image segmentation.

The proposed algorithm was evaluated using 39 AVMs. Our results demonstrated that automated segmentation using FCM has >70% sensitivity and specificity in the identification of AVM nidal composition. These are in reference to the results using manual segmentation, which depends on image clarity and could be subject to potential biases. Thus, whether manual clustering is more accurate than automated clustering remains open to debate. Currently, automated clustering can provide clinicians with a method to quantify the AVM nidal composition.

Stratification of Risk in the Post-ARUBA (A Randomized Trial of Unruptured Brain Arteriovenous Malformations) Era

The results of the present study are of particular importance in the context of the ongoing controversy pertaining to the management of unruptured AVMs. This issue is especially important because of the recent results from the ARUBA study (a randomized trial of unruptured brain arteriovenous malformations).[39] ARUBA study reported that intervention for unruptured cerebral AVMs carries a significantly elevated risk of morbidity compared with observation. However, in the post-ARUBA era and in the context of the results from the present study, we believe that patients with compact AVMs are still worthy candidates for SRS, our current management of unruptured brain AVMs. Considering the relatively benign nature of unruptured AVMs, the threshold for the brain tissue component should be lower than that for ruptured lesions. As demonstrated in the present study, the strict selection of patients could help to ensure that the administration of SRS for compact, unruptured AVMs would provide a high likelihood of nidal obliteration and a low risk of AREs.

Study Limitations

Our initial objective was to validate the proposed method; therefore, we enrolled only a small patient population. Thus, our study was prone to bias with regard to patient selection and treatment. In addition, our results are not necessarily applicable to extrasmall and extralarge AVMs. Finally, our data might have been contaminated in cases in which the AVM had occurred close to the scalp bone, with evidence of calcification and/or interference with AVM segmentation. More AVM cases and improved imaging resolution could increase the validation of the proposed method.

CONCLUSIONS

In the present study, a novel segmentation and unsupervised learning method was used to characterize the components within the AVM nidus and draw correlations with the occurrence of SRS complications. The percentage of brain tissue within the nidus was found to be associated with a greater incidence of RICs. Furthermore, the vascular component within the nidus was not found to be associated with AVM obliteration. The proposed automated segmentation scheme provides a tool by which to predict the degree of risk imposed by SRS in the treatment of brain AVMs.

ACKNOWLEDGMENTS

The authors would like to thank all the colleagues who contributed to the present study. We are grateful to our research assistants, Fong-Jiao Lee, Hsueh-Jen Huang, Wen-Chi Ku, Yi-Bei Tseng, and Lan Huang Jr. for their data recording and transcription. We thank the editor and series editor for constructive criticisms of an earlier version of our report.

REFERENCES

1. Kano H, Flickinger JC, Tonetti D, et al. Estimating the risks of adverse radiation effects after gamma knife radiosurgery for arteriovenous malformations. *Stroke*. 2017;48:84-90.
2. Ding D, Starke RM, Kano H, et al. Stereotactic radiosurgery for Spetzler-Martin grade III arteriovenous malformations: an international multicenter study. *J Neurosurg*. 2017;126:859-871.
3. Ding D, Yen CP, Xu Z, Starke RM, Sheehan JP. Radiosurgery for low-grade intracranial arteriovenous malformations. *J Neurosurg*. 2014;121:457-467.
4. Ding D, Yen CP, Xu Z, Starke RM, Sheehan JP. Radiosurgery for primary motor and sensory cortex arteriovenous malformations: outcomes and the effect of eloquent location. *Neurosurgery*. 2013;73:816-824 [discussion: 824].
5. Starke RM, Ding D, Kano H, et al. International multicenter cohort study of pediatric brain arteriovenous malformations. Part 2: outcomes after stereotactic radiosurgery. *J Neurosurg Pediatr*. 2017;19:136-148.

6. Ilyas A, Chen CJ, Ding D, et al. Radiation-induced changes after stereotactic radiosurgery for brain arteriovenous malformations: a systematic review and meta-analysis. *Neurosurgery*. 2018;83:365-376.

7. Ilyas A, Chen CJ, Ding D, et al. Cyst formation after stereotactic radiosurgery for brain arteriovenous malformations: a systematic review. *J Neurosurg*. 2018;128:1354-1363.

8. Aoyama H, Shirato H, Nishioka T, et al. Treatment outcome of single or hypofractionated single-isocentric stereotactic irradiation (STI) using a linear accelerator for intracranial arteriovenous malformation. *Radiother Oncol*. 2001;59:323-328.

9. Blamek S, Boba M, Larysz D, et al. The incidence of imaging abnormalities after stereotactic radiosurgery for cerebral arteriovenous and cavernous malformations. *Acta Neurochir Suppl*. 2010;106:187-190.

10. Ding D, Yen CP, Starke RM, Xu Z, Sheehan JP. Radiosurgery for ruptured intracranial arteriovenous malformations. *J Neurosurg*. 2014;121:470-481.

11. Ding D, Yen CP, Xu Z, Starke RM, Sheehan JP. Radiosurgery for patients with unruptured intracranial arteriovenous malformations. *J Neurosurg*. 2013;118:958-966.

12. Flickinger JC, Lunsford LD, Kondziolka D, et al. Radiosurgery and brain tolerance: an analysis of neurodiagnostic imaging changes after gamma knife radiosurgery for arteriovenous malformations. *Int J Radiat Oncol Biol Phys*. 1992;23:19-26.

13. Ganz JC, Reda WA, Abdelkarim K, Hafez A. A simple method for predicting imaging-based complications following gamma knife surgery for cerebral arteriovenous malformations. *J Neurosurg*. 2005;102(suppl):4-7.

14. Massengale JL, Levy RP, Marcellus M, Moes G, Marks MP, Steinberg GK. Outcomes of surgery for resection of regions of symptomatic radiation injury after stereotactic radiosurgery for arteriovenous malformations. *Neurosurgery*. 2006;59:553-560 [discussion: 553-560].

15. Steinberg GK, Chang SD, Levy RP, Marks MP, Frankel K, Marcellus M. Surgical resection of large incompletely treated intracranial arteriovenous malformations following stereotactic radiosurgery. *J Neurosurg*. 1996;84:920-928.

16. Bose R, Agrawal D, Singh M, et al. Draining vein shielding in intracranial arteriovenous malformations during gamma-knife: a new way of preventing post gamma-knife edema and hemorrhage. *Neurosurgery*. 2015;76:623-631 [discussion: 631-632].

17. Buis DR, Meijer OW, van den Berg R, et al. Clinical outcome after repeated radiosurgery for brain arteriovenous malformations. *Radiother Oncol*. 2010;95:250-256.

18. Han JH, Kim DG, Chung HT, et al. Clinical and neuroimaging outcome of cerebral arteriovenous malformations after gamma knife surgery: analysis of the radiation injury rate depending on the arteriovenous malformation volume. *J Neurosurg*. 2008;109:191-198.

19. Hayhurst C, Monsalves E, van Prooijen M, et al. Pretreatment predictors of adverse radiation effects after radiosurgery for arteriovenous malformation. *Int J Radiat Oncol Biol Phys*. 2012;82:803-808.

20. Huang PP, Rush SC, Donahue B, et al. Long-term outcomes after staged-volume stereotactic radiosurgery for large arteriovenous malformations. *Neurosurgery*. 2012;71:632-643 [discussion: 643-644].

21. Kiran NA, Kale SS, Kasliwal MK, et al. Gamma knife radiosurgery for arteriovenous malformations of basal ganglia, thalamus and brainstem—a retrospective study comparing the results with that for AVMs at other intracranial locations. *Acta Neurochir (Wien)*. 2009;151:1575-1582.

22. Miyawaki L, Dowd C, Wara W, et al. Five year results of LINAC radiosurgery for arteriovenous malformations: outcome for large AVMS. *Int J Radiat Oncol Biol Phys*. 1999;44:1089-1106.

23. Morikawa M, Numaguchi Y, Rigamonti D, et al. Radiosurgery for cerebral arteriovenous malformations: assessment of early phase magnetic resonance imaging and significance of gadolinium-DTPA enhancement. *Int J Radiat Oncol Biol Phys*. 1996;34:663-675.

24. Parkhutik V, Lago A, Aparici F, et al. Late clinical and radiological complications of stereotactical radiosurgery of arteriovenous malformations of the brain. *Neuroradiology*. 2013;55:405-412.

25. Ilyas A, Chen CJ, Ding D, et al. Volume-staged versus dose-staged stereotactic radiosurgery outcomes for large brain arteriovenous malformations: a systematic review. *J Neurosurg*. 2018;128:154-164.

26. Moosa S, Chen CJ, Ding D, et al. Volume-staged versus dose-staged radiosurgery outcomes for large intracranial arteriovenous malformations. *Neurosurg Focus*. 2014;37:E18.

27. Flickinger JC, Kondziolka D, Lunsford LD, et al. Development of a model to predict permanent symptomatic postradiosurgery injury for arteriovenous malformation patients. Arteriovenous Malformation Radiosurgery Study Group. *Int J Radiat Oncol Biol Phys*. 2000;46:1143-1148.

28. Guo WY, Lee SM, Chang YC, Pan HC. The impact of arteriovenous malformation radiosurgery on the brain: From morphology and perfusion to neurocognition. *Stereotact Funct Neurosurg*. 2006;84:162-169.

29. Lee CC, Pan DH, Ho DM, et al. Chronic encapsulated expanding hematoma after gamma knife stereotactic radiosurgery for cerebral arteriovenous malformation. *Clin Neurol Neurosurg*. 2011;113:668-671.

30. Lee CC, Reardon MA, Ball BZ, et al. The predictive value of magnetic resonance imaging in evaluating intracranial arteriovenous malformation obliteration after stereotactic radiosurgery. *J Neurosurg*. 2015;123:136-144.

31. Lin CJ, Yang HC, Chien AC, et al. In-room assessment of intravascular velocity from time-resolved rotational angiography in patients with arteriovenous malformation: a pilot study. *J Neurointerv Surg*. 2018;10:580-586.

32. Yen CP, Matsumoto JA, Wintermark M, et al. Radiation-induced imaging changes following gamma knife surgery for cerebral arteriovenous malformations. *J Neurosurg*. 2013;118:63-73.

33. Bezdek JC, Ehrlich R, Full W. FCM: The fuzzy c-means clustering algorithm. *Comput Geosci*. 1984;10:191-203.

34. Ji ZX, Sun QS, Xia DS. A modified possibilistic fuzzy c-means clustering algorithm for bias field estimation and segmentation of brain MR image. *Comput Med Imaging Graph*. 2011;35:383-397.

35. Shuto T, Yagishita S, Matsunaga S. Pathological characteristics of cyst formation following gamma knife surgery for arteriovenous malformation. *Acta Neurochir (Wien)*. 2015;157:293-298.

36. Schneider BF, Eberhard DA, Steiner LE. Histopathology of arteriovenous malformations after gamma knife radiosurgery. *J Neurosurg*. 1997;87:352-357.

37. Szeifert GT, Kemeny AA, Timperley WR, Forster DM. The potential role of myofibroblasts in the obliteration of arteriovenous malformations after radiosurgery. *Neurosurgery*. 1997;40:61-65 [discussion: 65-66].

38. Rahmathulla G, Marko NF, Weil RJ. Cerebral radiation necrosis: a review of the pathobiology, diagnosis and management considerations. *J Clin Neurosci*. 2013;20:485-502.

39. Mohr JP, Parides MK, Stapf C, et al. Medical management with or without interventional therapy for unruptured brain arteriovenous malformations (ARUBA): a multicentre, non-blinded, randomised trial. *Lancet*. 2014;383:614-621.

Conflict of interest statement: This work was partly supported by the Ministry of Science and Technology, Taiwan (project no. 105-2314-B-075-021, 107-2221-E-009-103) and partly supported by the Center for Neuromodulation Medical Electronics Systems from the Featured Areas Research Center Program within the framework of the Higher Education Sprout Project by the Ministry of Education in Taiwan.

Received 2 October 2018; accepted 29 December 2018

Citation: World Neurosurg. (2019) 125:e132-e138.
https://doi.org/10.1016/j.wneu.2018.12.220

Journal homepage: ***www.journals.elsevier.com/world-neurosurgery***

Available online: ***www.sciencedirect.com***